



Numerical Study on the Magnetohydrodynamics of a Liquid Metal Oscillatory Flow under Inductionless Approximation

J. A. Rizzo-Sierra

Applied Science and Advanced Technology Research Center, National Polytechnic Institute, (CICATA-IPN), Santiago de Querétaro, Querétaro, 76090, México

Email: amilcar.rizzo@gmail.com

(Received November 12, 2015; accepted January 13, 2016)

ABSTRACT

A harmonically-driven, incompressible, electrically conducting, and viscous liquid metal magnetohydrodynamic flow through a thin walled duct of rectangular cross section interacting with a uniform magnetic field traverse to its motion direction is numerically investigated. Chebyshev spectral collocation method is used to solve the Navier-Stokes equation under the inductionless approximation for the magnetic field in the gradient formulation for the electric field. Flow is considered fully developed in the direction perpendicular to the applied magnetic field and laminar in regime. Validation of numerical calculations respect to analytical calculations is established. Flow structure and key magnetohydrodynamic features regarding eventual alternating power generation application in a rectangular channel liquid metal magnetohydrodynamic generator setup are numerically inquired. Influence of pertinent parameters such as Hartmann number, oscillatory interaction parameter and wall conductance ratio on magnetohydrodynamic flow characteristics is illustrated. Particularly, it is found that in the side layer and its vicinity the emerging flow structures/patterns depend mainly on the Hartmann number and oscillatory interaction parameter ratio, while the situation for the Hartmann layer and its vicinity is less eventful. A similar feature has been discussed in the literature for the steady liquid metal flow case and served as rationale for developing the composite core-side-layer approximation to study the magnetohydrodynamics of liquid metal flows usable in direct power generation. In this study that approximation is not considered and the analysis is performed on liquid metal oscillatory (i., e., unsteady) flows usable in alternating power generation. Conversely, in terms of prospective practical applicability the formulation developed and tested with these calculations admits the implementation of a load resistance and walls conductivity optimization. That means that besides representing a numerical study on the magnetohydrodynamics of the oscillatory flow under consideration, absent in the literature for the parametric ranges reported, the formulation presently implemented can also be applicable to study the performance of an alternating liquid metal magnetohydrodynamic generator in the rectangular channel configuration.

Keywords: Magnetohydrodynamics; Oscillatory liquid metal flow; Laminar fully developed regime; Inductionless approximation; Navier-Stokes equation; Spectral collocation method; Power generation.

NOMENCLATURE

a, b	duct's semi height, semi width	L	a characteristic length for the problem
B_0	applied magnetic field magnitude	M	Hartmann's number
\bar{B}	applied magnetic field	N_w	oscillatory interaction parameter
$\mathbb{C}_H, \mathbb{C}_L$	Hartmann, side wall conductance ratios	∇p	pressure gradient
d	duct's wall thickness	\vec{u}	velocity field
\bar{E}	electric field	u_0^*	a characteristic velocity for the problem
\bar{f}	Lorentz force	R_m	Reynolds number
G	pressure gradient amplitude	R_ω	magnetic R
i	imaginary unit	R_ω	oscillatory Reynolds number
\bar{J}	electric current density	t	time variable

ν	fluid's kinematic viscosity	σ_H, σ_L	Hartmann, side wall electric conductivities
ν_m	fluid's magnetic permeability	ϕ	electric potential
ρ	fluid's volumetric density	ω	angular frequency
σ	fluid's electric conductivity		

1. INTRODUCTION

Of interest to this paper is the characterization of MHD flows occurring in ducts or channels interacting with moderate to high intensity magnetic fields. Apart from the purely the physical interest of the subject, characterizing MHD flows is important within the contexts of nuclear power generation (e. g., liquid metal based cooling systems), alternative power generation/conversion (e. g., liquid metal magnetohydrodynamic -LMMHD- electric generators/converters), and industrial liquid metal or conductive fluids transport and handling (e. g., accelerators, pumps, flow meters). In general, the analytical/theoretical treatment of MHD duct flow problems is difficult due to the coupling of equations of fluid mechanics and electrodynamics. Because of that, exact analytical solutions are only available for relatively straightforward geometries subject to simple boundary conditions. Over time a range of numerical techniques have been used to solve MHD duct flow problems, such as finite difference method (FDM), finite element method (FEM), finite volume method (FVM), boundary element method (BEM), and spectral collocation methods (SCM). Examples of the first two can be found in Singh and Lal (1978), (1979), (1984), where numerical solutions of MHD duct flows through different cross-sections were obtained for Hartmann numbers of $O(\leq 10^1)$. Gardner and Gardner (1995) also applied FEM using bicubic B-spline elements for Hartmann numbers of the same order of magnitude, study which was taken further by Tezer-Sezgin and Köksal (1989) up to moderate Hartmann numbers of $O(\leq 10^2)$ using linear and quadratic element based (FEM). Demendy and Nagy (1997) used analytical (FEM) methodology to obtain numerical solutions for Hartmann numbers of $O(\leq 10^3)$. Barrett (2001) also used this methodology to obtain solutions for high M values, reporting increasingly high computational costs. Nesliturk and Tezer-Sezgin (2005), (2006) solved the MHD duct flow equations for rectangular cross-sections using another (FEM) based technique called stabilized (FEM) with residual free bubble functions, reporting huge computational costs too. Now, the use of (BEM) based methods has been favored as a way to deal with the difficulties of managing large system sizes due to the need to increase domain discretization accuracy. Examples for Hartmann numbers of $O(\leq 10^1)$ are given by Singh and Agarwal (1984), Tezer-Sezgin (1994), Liu and Zhu (2002), Tezer-Sezgin and Aydın (2002), Carabineanu *et al.* (1995), and Bozkaya and Tezer-Sezgin (2006). Particularly, Liu and Zhu (2002), and Bozkaya and Tezer-Sezgin (2008),

applied a (BEM) based methodology variant referred as dual reciprocity boundary element method (DRBEM) for non-conducting walls, and also another one referred as time-domain (BEM) for arbitrary wall conductivity unsteady MHD duct flow. Tezer-Sezgin and Aydın (2006) obtained results for Hartmann numbers of $O(\leq 10^2)$ using constant boundary elements. Bozkaya and Tezer-Sezgin (2007) worked up a root solution to the (BEM) solution of MHD insulated and partly insulated wall duct problem for Hartmann numbers of $O(\leq 10^2)$. Dehghan and Mirzaei (2009) proposed a technique referred as meshless local boundary integral equation method (LBIE) in order to obtain numerical solutions for coupled velocity and magnetic field equations for unsteady MHD rectangular and circular cross-sectioned duct flows with non-conducting walls. On the other hand, spectral collocation based methods have been used in pure and applied mathematics, e., g., Sezer and Kaynak (1996), Akyüz and Sezer (2003), Akyüz-Daşcıoğlu and Sezer (2005), Çelik (2005a), Çelik (2005b), Çelik and Gokmen (2005), Çelik (2006), Keşan (2003), but also in MHD duct flow problems for the coupled steady case by Çelik (2011) and in the inductionless approach for the steady case by Cuevas *et al.* (1997). A combination of finite volume element method and spectral method is proposed in Shakeri and Dehghan (2011) for the coupled velocity and magnetic field rectangular cross-section unsteady case, focusing on building up and evaluating the method viability in terms of correctly combining the two techniques and establishing its validation respect to available analytical solutions as well as numerical ones for Hartmann numbers of $O(\leq 10^2)$. In general, when applicable spectral collocation methods are found to be very practical in terms of solid convergence towards solutions behavior and overall computational efficiency. Regarding the subject of oscillatory MHD duct flows, precedent works include Mehmood and Ali (2007), who analytically investigated an oscillatory MHD porous filled duct flow linking the possible effects of heat and vibration transfer respect to boundary condition compliance. Mandal developed a detailed analytical treatment of an oscillatory MHD flow through a rectangular cross-sectioned duct. His approach regards isolating walls parallel to the applied magnetic field (also referred as side or lateral walls) and thin arbitrary conducting walls perpendicular to the field (also referred as Hartmann walls) in Mandal (1968); and thin arbitrary conducting side walls and perfectly conducting Hartmann walls in Mandal (1969). Additional examples of analytical treatment for MHD duct flow problems can be found in Shercliff (1953), Chang and Lundgren (1961), Hunt

(1965), Hunt and Stewartson (1965).

In this paper the (SCM) based upon the work of Cuevas (1994), Cuevas *et al.* (1997) for the steady MHD duct flow case is used to develop a numerical study on a family of oscillatory flows potentially useful in alternating power generation. Formulation here implemented allows considering independent thin conducting side and Hartmann walls including the insulating and perfectly conducting limit cases; but here we restrict ourselves to both thin side and Hartmann walls of equal conductivity under validity conditions for thin wall approximation as established in Cuevas (1994), Cuevas *et al.* (1997), case which isn't covered in Mandal (1968), Mandal (1969). The paper is organized as follows. The problem is physically formulated in section 2 below. In section 3, a brief summary on the employed spectral collocation numerical formulation is given. In section 4, a comparison between our numerical solution and an unrestricted analytical solution obtained for isolating side walls and perfectly conducting Hartmann walls ($C_L = 0, C_H \rightarrow \infty$) is presented. In section 5, numerical results on the velocity profiles and electric current are presented and discussed in terms of the dimensionless parameters defining the problem. Concluding remarks are given in section 6. Finally, Appendix A gives further details on the obtention procedure of the analytical solution used in section 4.

2. PHYSICAL FORMULATION

Consider a harmonically-driven, incompressible, electrically conducting, laminar, completely developed, and viscous flow through a thin walled duct of rectangular cross section interacting with an uniform magnetic field traverse to its motion direction. Basic schematic of the situation is presented in Fig. 1. Under these circumstances, functional dependence in the Cartesian coordinate system of all variables lies in y, z and t coordinates. $\vec{u} = u_x(x, y, z)\hat{e}_x$ defines the velocity field, where \hat{e}_x is the unit vector in x direction. Conductivity of Hartmann walls (perpendicular to the applied magnetic field) is not necessarily the same as the one of the side walls (parallel to the applied magnetic field).

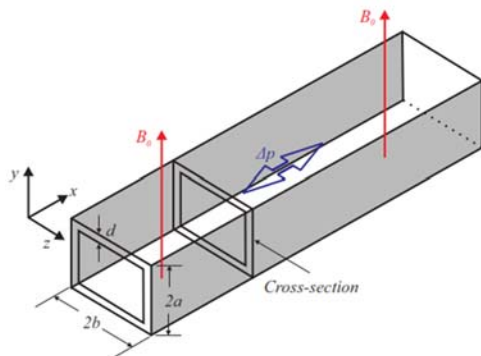


Fig. 1. Schematic of the problem.

Solving the Navier-Stokes equation gives the velocity vector field:

$$\frac{\partial \vec{u}}{\partial t} + (\vec{u} \cdot \nabla) \vec{u} = -\frac{1}{\rho} \nabla p + \nu \nabla^2 \vec{u} + \frac{\vec{f}}{\rho} \quad (1)$$

Where $p = p(x, t)$ and its gradient ∇p relate to the functional dependence of the pressure applied to the fluid, \vec{B} is the applied homogeneous magnetic field, $\vec{f} = \vec{j} \times \vec{B}$ is the electromagnetic body force in the fluid, related to \vec{j} , the induced electric current, which in its turn is given by Ohm's law for a moving medium:

$$\vec{j} = \sigma (\vec{E} + \vec{u} \times \vec{B}) \quad (2)$$

On the other hand, ρ is the fluid's volumetric mass density and ν its kinematic viscosity. If the flow is assumed slow enough, the induced magnetic field can be considered negligible compared to the externally imposed one. That constitutes the inductionless approximation, which can be expressed as $R_m = \nu_m \sigma u_0^* L \ll 1$. R_m is defined as the magnetic Reynolds number, a conventional MHD dimensionless parameter which represents the ratio between induction and diffusion of the magnetic field in a given situation. ν_m , σ , are the fluid's magnetic permeability and electrical conductivity while u_0^* , L are respectively one characteristic velocity and length for the problem. Furthermore, if we reinterpret the inductionless approximation in terms of the much shorter time scale of magnetic field diffusion compared to that of velocity field variation, the quasistationary approximation yielding to $\vec{E} = -\nabla \phi$ is properly called for. $\phi = \phi(x, y, z)$ is the electrostatic potential.

Using Ohm's law in the form $\vec{j} = \sigma (-\nabla \phi + \vec{u} \times \vec{B})$, Eq. (2) turns into:

$$\vec{j} = \sigma \left(-\frac{\partial \phi}{\partial y} \hat{y} - \frac{\partial \phi}{\partial z} \hat{z} + u B_0 \hat{z} \right) \quad (3)$$

With it, the electromagnetic body force in Eq. (1) assumes the form:

$$\frac{\vec{f}}{\rho} = \sigma \left(-\frac{\partial \phi}{\partial y} \hat{y} - \frac{\partial \phi}{\partial z} \hat{z} + u B_0 \hat{z} \right) \times B_0 \hat{y} \quad (4)$$

Replacing Eq. (4) into Eq. (1), one obtains:

$$\frac{\partial u}{\partial t} = -\frac{1}{\rho} \frac{\partial p}{\partial x} + \nu \left(\frac{\partial^2 u}{\partial y^2} + \frac{\partial^2 u}{\partial z^2} \right) - \frac{B_0}{\rho} j_z \quad (5)$$

Proposing the adimensionalization given by $\tilde{B} = B / B_0 = 1$,

$\tilde{u} = u / u_0^*$, $\tilde{y} = y / L$, $\tilde{z} = z / L$, $\tilde{d} = d / L$, Eq. (5) conduces whether to:

$$N_\omega^{-1} \frac{\partial \tilde{u}}{\partial \tilde{t}} = -\frac{\partial \tilde{p}}{\partial \tilde{x}} + M^{-2} \left(\frac{\partial^2 \tilde{u}}{\partial \tilde{y}^2} + \frac{\partial^2 \tilde{u}}{\partial \tilde{z}^2} \right) - \tilde{j}_z \quad (6)$$

Or

$$R_\omega \frac{\partial \tilde{u}}{\partial \tilde{t}} = -M^2 \frac{\partial \tilde{p}}{\partial \tilde{x}} + \left(\frac{\partial^2 \tilde{u}}{\partial \tilde{y}^2} + \frac{\partial^2 \tilde{u}}{\partial \tilde{z}^2} \right) - M^2 \tilde{j}_z \quad (7)$$

According to the set of dimensionless parameters chosen to define the problem. $M^2 = N_\omega R_\omega$ establishes the relation between the parameters. $M \equiv B_0 L \sqrt{\sigma / \rho \nu}$ is the Hartmann number, which represents the ratio of electromagnetic to viscous forces in the problem, $N_w \equiv \sigma B_0^2 / \rho \omega$ is the oscillatory interaction parameter, representing the ratio of electromagnetic to inertial forces, and $R_\omega = \omega L^2 / \nu$ is the oscillatory Reynolds number, representing the ratio of inertial to viscous forces. Choosing Eq. (6), to solve it we propose all variables to be harmonically dependent on time as follows:

$$\left\{ \begin{array}{l} \tilde{u} \\ \tilde{\phi} \\ \tilde{\phi}_w \\ \tilde{p} \\ \partial \tilde{p} / \partial \tilde{x} \\ \tilde{j}_y \\ \tilde{j}_z \\ \tilde{j}_{yw} \\ \tilde{j}_{zw} \end{array} \right\} = \Re \left\{ \begin{array}{l} \tilde{u}_0(\tilde{y}, \tilde{z}) \\ \tilde{\phi}_0(\tilde{y}, \tilde{z}) \\ \tilde{\phi}_{0w}(\tilde{y}, \tilde{z}) \\ \tilde{p}_0(\tilde{x}) \\ \tilde{G} \\ \tilde{j}_{y0}(\tilde{y}, \tilde{z}) \\ \tilde{j}_{z0}(\tilde{y}, \tilde{z}) \\ \tilde{j}_{y0w}(\tilde{y}, \tilde{z}) \\ \tilde{j}_{z0w}(\tilde{y}, \tilde{z}) \end{array} \right\} e^{i\tilde{t}} \quad (8)$$

From top to bottom: velocity field, fluid region electric potential, wall region electric potential, pressure, gradient pressure (is the pressure gradient amplitude and $\partial \tilde{p} / \partial \tilde{x} = (1 / \sigma B_0^2 u_0^*) \partial p / \partial x$ its adimensionalization equation), fluid region surface electric current density y component, fluid region surface electric current density z component, wall region surface electric current density y component, wall region surface electric current density z component. \Re means taking the real part as physically meaningful. Replacing pertinent quantities into Eq. (6), one obtains a complex variable equation independent of time for the fluid region:

$$M^{-2} \left(\frac{\partial^2 \tilde{u}_0}{\partial \tilde{y}^2} + \frac{\partial^2 \tilde{u}_0}{\partial \tilde{z}^2} \right) - \tilde{j}_{z0} - i N_\omega^{-1} \tilde{u}_0 = \tilde{G} \quad (9)$$

Variables with tildes are dimensionless, and from now on that notation will be dropped since dimensionless quantities will be assumed by implication. As stated, the solution for the velocity field will be the real part of $u = u_0(y, z)e^{it}$. Charge conservation in the problem, expressed as $\nabla \cdot \vec{J} = 0$ implies that:

$$j_{yo} = -\frac{\partial \phi_0}{\partial y}, \quad j_{zo} = -\frac{\partial \phi_0}{\partial z} + u_0 \quad (10)$$

$$\frac{\partial j_{yo}}{\partial y} + \frac{\partial j_{zo}}{\partial z} = 0 \quad (11)$$

$$j_{yow} = -\left(\frac{\sigma_H}{\sigma} \right) \frac{\partial \phi_{0w}}{\partial y}, \quad j_{zow} = -\left(\frac{\sigma_L}{\sigma} \right) \frac{\partial \phi_{0w}}{\partial z} \quad (12)$$

$$\frac{\partial j_{y0w}}{\partial y} + \frac{\partial j_{z0w}}{\partial z} = 0 \quad (13)$$

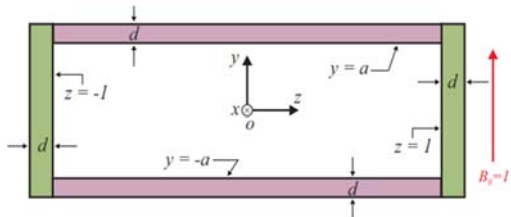


Fig. 2. Duct dimensionless cross-section.

$\sigma_H / \sigma = C_H / d$ and $\sigma_L / \sigma = C_L / d$. C_H and C_L are defined as conductance ratios for Hartmann and side walls respectively. It should be noticed that these quantities are dimensionless from definition. The problem is then defined by Eqs. (9) to (13), but further considerations must be made to complete its physical formulation. No initial conditions are required since presently we are not interested in the transient solution, so focus is put on boundary conditions. Departing from considering symmetry in both y and z directions with $b = 1$ (shown in Fig. 2), a complete reformulation to the problem can be developed based on the work by Cuevas (1994) and Cuevas *et al.* (1997) for the steady case, in order to advance the following steps into obtaining a solution. First, define pertinent to the case and proper hydrodynamic and electromagnetic boundary conditions within fluid, wall and outer regions. Second, exploiting the fact that the electric current is divergence free and two dimensional (2-D) —see again Eqs. (10)-(13)—, propose for them properly defined fluid and wall regions electric current stream functions. Third, decouple the resulting equations within fluid region from those within wall and outer regions by forwarding a potential function in terms of both the fluid region electric current stream function and electric potential; then applying for it the thin wall approximation, i. e., regarding $d \ll 1$ and the medium around the duct (outer region) as fully isolating. d is the width of the duct walls, as shown in Fig. 2. These steps have the overall effect of rendering the system given by Eqs. (9)-(13) into a single variable within the fluid region, i. e., $F = F(y, z)$. Since that reformulation is based on what was developed in those references, no further details are necessary here. Previous considerations conduce to the following set of equations and boundary conditions defining our problem:

- a) Fluid region governing equation.

$$M^{-2} \left(\frac{\partial^2 u_0}{\partial y^2} + \frac{\partial^2 u_0}{\partial z^2} \right) - \frac{\partial^2 F}{\partial y^2} - iN_\omega^{-1} u_0 = G \quad (14)$$

Where, given that $0 < y < a \wedge 0 < z < 1$:

$$u_0 = \frac{\partial^2 F}{\partial y^2} + \frac{\partial^2 F}{\partial z^2} \quad (15)$$

b) Boundary conditions. At $z = 0$:

$$\frac{\partial}{\partial z} \left(\frac{\partial^2 F}{\partial y^2} + \frac{\partial^2 F}{\partial z^2} \right) = 0, \quad \frac{\partial F}{\partial z} = 0 \quad (16)$$

At $y = 0$:

$$\frac{\partial}{\partial y} \left(\frac{\partial^2 F}{\partial y^2} + \frac{\partial^2 F}{\partial z^2} \right) = 0, \quad \frac{\partial F}{\partial y} = 0 \quad (17)$$

$$\left(\frac{\partial^2 F}{\partial y^2} + \frac{\partial^2 F}{\partial z^2} \right) = 0, \quad F + C_L \frac{\partial F}{\partial z} = 0 \quad (18)$$

At $y = a$

$$\left(\frac{\partial^2 F}{\partial y^2} + \frac{\partial^2 F}{\partial z^2} \right) = 0, \quad \frac{\partial F}{\partial y} - (C_H + M^{-1}) \frac{\partial^2 F}{\partial z^2} = M^{-1} \frac{\partial^2 F}{\partial y^2} \quad (19)$$

In addition to what is conditioned by means of Eqs. (14) to (19), the physical formulation must also take into account the dimensionless volumetric flow conservation condition in terms of the averaged velocity amplitude (u_0):

$$\int_0^a \int_0^1 u_0 dy dz = a \quad (20)$$

Eq. (20) comes from $\int_{ds} \bar{u}_0 \bar{ds} = \int_0^a \int_0^1 u_0 dy dz = a$,

since a is simultaneously the duct cross section dimensionless area and aspect ratio. Because the spatial average of u_0 is $\langle u_0 \rangle = \int_{ds} \bar{u}_0 \bar{ds} / \int ds$, in

order to normalize u respect to it one has:

$$u_n = \frac{u(y, z, t)}{\langle u_0 \rangle} = a \frac{u_0(y, z) e^{it}}{\int_0^a \int_0^1 u_0 dy dz} \quad (21)$$

3. NUMERICAL FORMULATION

To solve Eqs. (14)-(19) by means of the spectral collocation method, a function $F = F(y, z)$ satisfying the boundary conditions is proposed as a finite series of even Chebyshev polynomials ($T_{2m}(y/a)$, and $T_{2n}(z)$):

$$F(y, z) = \sum_{m=0}^{N_y} \sum_{n=0}^{N_z} A_{mn} T_{2m} \left(\frac{y}{a} \right) T_{2n}(z) \quad (22)$$

Variables to determine are the complex coefficients A_{mn} . N_y and N_z the number of terms taken along y coordinate and z coordinate respectively. Use of the Gauss-Lobatto collocation points set is convenient because it yields the appropriate numerical resolution for the boundary layers by concentrating the points near the walls. The unknown coefficients can be considered as a vector $\beta(AJ) = A_{mn}$, and the algebraic system of simultaneous equations can be expressed as:

$$\sum_{AJ=1}^{N_T} \alpha_{PJ \times AJ} \beta_{AJ} = \gamma_{PJ} \quad (23)$$

Where $AJ = m(N_z + 1) + n + 1, 1 \leq PJ \wedge AJ \leq N_T$, and $N_T = (N_y + 1)(N_z + 1)$. Elements of matrix $\alpha_{PJ \times AJ}$ and known vector γ_{PJ} are obtained by replacing Eq. (22) into Eqs. (14)-(19). Explicitly, into governing Eq. (14):

$$\begin{aligned} & \sum_{m=0}^{N_y} \sum_{n=0}^{N_z} \left[\frac{1}{a^4} \frac{\partial^4 T_{2m} \left(\frac{y}{a} \right)}{\partial y^4} T_{2n}(z) \right. \\ & + \frac{2}{a^2} \frac{\partial^2 T_{2m} \left(\frac{y}{a} \right)}{\partial y^2} \frac{\partial^2 T_{2n}(z)}{\partial z^2} \\ & + T_{2m} \left(\frac{y}{a} \right) \frac{\partial^4 T_{2n}(z)}{\partial z^4} \\ & - \frac{M^2}{a^2} \frac{\partial^2 T_{2m} \left(\frac{y}{a} \right)}{\partial y^2} T_{2n}(z) \\ & - i \frac{M^2 N_\omega^{-1}}{a^2} \frac{\partial^2 T_{2m} \left(\frac{y}{a} \right)}{\partial y^2} T_{2n}(z) \\ & \left. - i M^2 N_\omega^{-1} T_{2m} \left(\frac{y}{a} \right) \frac{\partial^2 T_{2n}(z)}{\partial z^2} \right] A_{mn} \\ & = M^2 G \end{aligned} \quad (24)$$

When replacing into Eqs. (16) and (17), boundary conditions at $z = 0$ and $y = 0$ are identically satisfied, so no equations are generated. Into Eq. (18) left, the hydrodynamic boundary condition at $z = 1$ results:

$$\sum_{m=0}^{N_y} \sum_{n=0}^{N_z} \left[\frac{1}{a^2} \frac{\partial^2 T_{2m} \left(\frac{y}{a} \right)}{\partial y^2} + \frac{4n^2}{3} (4n^2 - 1) T_{2m} \left(\frac{y}{a} \right) \right] A_{mn} = 0 \quad (25)$$

Into Eq. (18) right, electromagnetic boundary condition at $z = 1$ results:

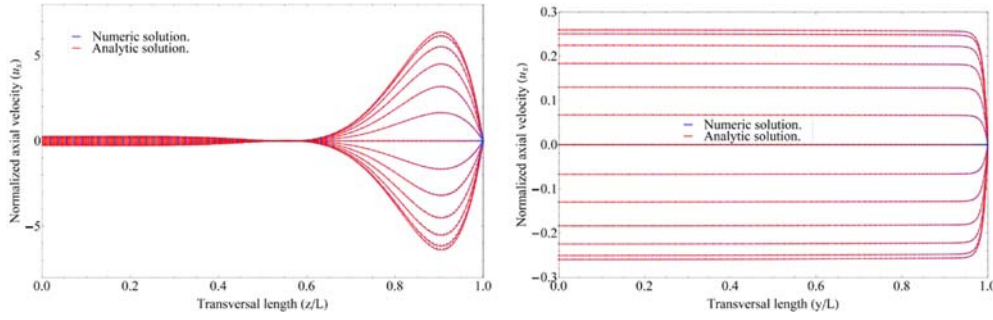


Fig. 3. Collocation vs. analytical solution at a moderate Hartmann number (M) and high interaction parameter (N_ω). $M = 102$, $N_\omega = 10^6$, and $t = 0 - \pi$ Rads in increments of $\pi/12$ Rads. $C_L = 0$, $C_H \rightarrow \infty$, $a = 1$. Left: profiles at $y = 0$. Right: profiles at $z = 0$.

$$\sum_{m=0}^{N_y} \sum_{n=0}^{N_z} \left(T_{2m} \left(\frac{y}{a} \right) + 4n^2 C_L T_{2m} \left(\frac{y}{a} \right) \right) A_{mn} = 0 \quad (26)$$

Into Eq. (19) left, the hydrodynamic boundary condition at $y = a$ results:

$$\sum_{m=0}^{N_y} \sum_{n=0}^{N_z} \left(\frac{4m^2}{3a^2} (4m^2 - 1) T_{2n}(z) + \frac{\partial^2 T_{22}(z)}{\partial z^2} \right) A_{mn} = 0 \quad (27)$$

Into Eq. (19), the electromagnetic boundary condition at $y = a$ results:

$$\sum_{m=0}^{N_y} \sum_{n=0}^{N_z} \left(\frac{4m^2}{a} T_{2n}(z) + (C_H + M^{-1}) \frac{\partial^2 T_{2n}(z)}{\partial z^2} - \frac{4m^2 M^{-1} (4m^2 - 1)}{3a^2} T_{2n}(z) \right) A_{mn} = 0 \quad (28)$$

The system of linear simultaneous equations in the variables A_{mn} given by Eqs. (24)-(28) can be solved by Gauss-Jordan elimination or another suitable method. Once done that, the solution as proposed in Eq. (22) can be constructed.

4. ANALYTICAL VS. NUMERICAL COMPARISON

In absence of experimental data, numerical calculations are validated if they can get reasonably close to analytical results. An instance of validation is then provided by comparing numerical results with analytical solutions for the oscillatory flow case, as shown in Fig. 3 (left) and (right). This was performed by obtaining an analytical solution for isolating side walls and perfectly conducting Hartmann walls $C_L = 0, C_H \rightarrow \infty$ at a moderate Hartmann number, case which was also treated in Mandal (1969) but restricted there to obtaining an asymptotic approximation solution valid for large Hartmann numbers. The unrestricted analytical solution presented here was reached by means of the

separation of variables technique in the potential formulation for the problem (ϕ -formulation), see Appendix A for details. Dimensionless solution reads:

$$u(x, y, z) = \frac{\delta e^{-y(\sqrt{\varepsilon_1} + \sqrt{\varepsilon_2})}}{8\pi\gamma(2n+1)\varepsilon} \left(e^{\zeta_1 y} (\varepsilon_1((2\pi n + \pi)^2 - 2\varepsilon_2)) \right. \\ \left. (e^{\sqrt{2}y\sqrt{\varepsilon_2}} + 1) \operatorname{sech}(a\zeta_2) + 4(2\pi n + \pi)^2 \varepsilon e^{\zeta_2 y} \right) \\ - \varepsilon_2((2\pi n + \pi)^2 - 2\varepsilon_1) e^{\zeta_2 y} (e^{\sqrt{2}y\sqrt{\varepsilon_1}} + 1) \operatorname{sech}(a\zeta_1) \\ \left. \cos(\alpha_n z) e^{it} \right) \quad (29)$$

u being the magnitude of the velocity field, with the following dimensionless parameters/constants:

$$\eta = 1 + iN_\omega^{-1}, \quad \beta = \eta M^2 + \alpha_n^2, \quad \gamma = (1 - \eta)M^2 \alpha_n^2 - \alpha_n^4, \\ \delta = GM^2 \alpha_n \alpha_n, \quad \varepsilon = \sqrt{\beta^2 + 4\gamma}, \quad \varepsilon_1 = \beta + \varepsilon, \quad \zeta_1 = \\ \sqrt{\varepsilon_1} / \sqrt{2}, \quad \text{and} \quad \zeta_2 = \sqrt{\varepsilon_2} / \sqrt{2}.$$

5. RESULTS

Once found that numerical results are close to analytical results, a picture of the flow dynamics and structure is captured by a parametric study in terms of Hartmann number (M), oscillatory interaction parameter (N_ω), and in a first case the consideration of a single wall conductance ratio, i. e., $C_H = C_L = C$. Emphasis was put on M as high as possible because they are characteristic of strong applied magnetic fields, typical in electric generation applications. The range of N_ω was chosen primarily due to our interest in the flow at the low frequencies case having in mind liquid metal MHD generators. Finally, regarding C , values 0.0, 0.001, 0.01, and 0.05 were chosen due to interest in taking into account the transition from thin conducting to the insulating wall case. The number of collocation points to use for the obtention of a numerically stable collocation solution is a subtle topic. Generally speaking, considering the oscillatory case on its own on this particular subject is a self contained matter of

Table 1 M/N_ω and $NY = NZ$, for the set of numerical experiments performed

$N_\omega \downarrow, M \rightarrow$	10^0	10^1	10^2	10^3	10^4
10^0	$10^0, 85$	$10^1, 105$	$10^2, 125$	$10^3, 155$	$10^4, 210$
10^1	$10^{-1}, 85$	$10, 105$	$10^1, 125$	$10^2, 155$	$10^3, 210$
10^2	$10^{-2}, 85$	$10^{-1}, 105$	$10^0, 125$	$10^1, 155$	$10^2, 210$
10^3	$10^{-3}, 85$	$10^{-2}, 105$	$10^{-1}, 125$	$10^0, 155$	$10^1, 210$
10^4	$10^{-4}, 85$	$10^{-3}, 105$	$10^{-2}, 125$	$10^{-1}, 155$	$10^0, 210$
10^5	$10^{-5}, 85$	$10^{-4}, 105$	$10^{-3}, 125$	$10^{-2}, 155$	$10^{-1}, 210$
10^6	$10^{-6}, 85$	$10^{-5}, 105$	$10^{-4}, 125$	$10^{-3}, 155$	$10^{-2}, 210$

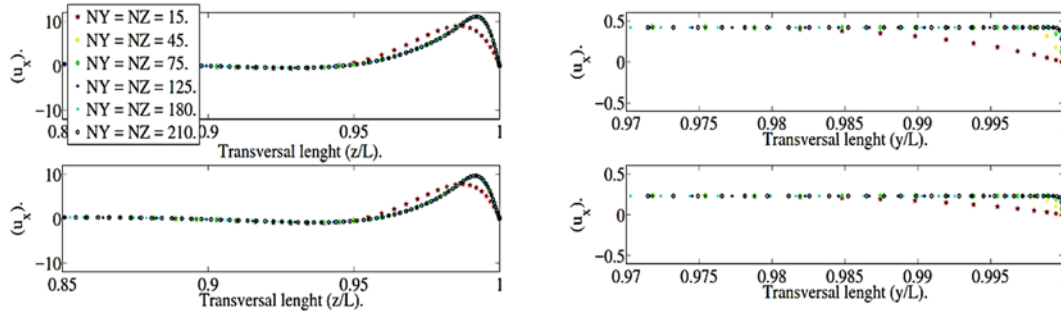


Fig. 4. Numerical solution respect to collocation parameters. $C = 0.05$, $N_\omega = 10^3$, $M = 10^4$, $M/N_\omega = 10$. $t = 4\pi/12$ (top) and $5\pi/12$ (Bottom)Rads. Left: profiles at $y = 0$. Right: profiles at $z = 0$.

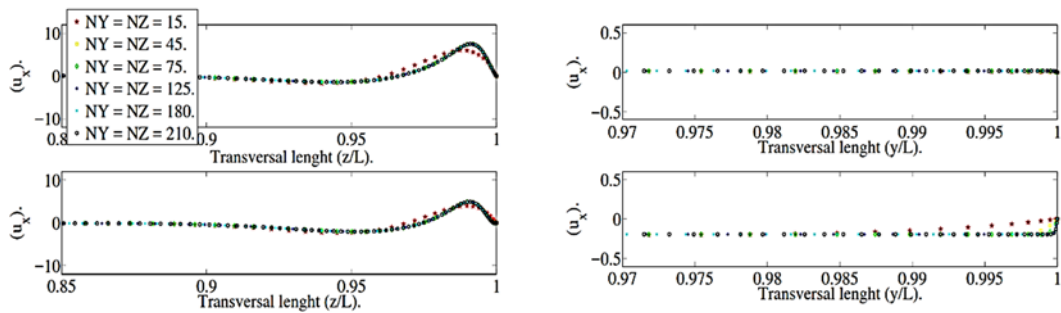


Fig. 5. Numerical solution respect to collocation parameters. $C = 0.05$, $N_\omega = 10^3$, $M = 10^4$, $M/N_\omega = 10$. $t = 6\pi/12$ (top) and $7\pi/12$ (Bottom)Rads. Left: profiles at $y = 0$. Right: profiles at $z = 0$.

inquiry since it varies in terms of both increasing M and M/N_ω . A picture of the situation is grasped with Table 5. filled with values of M/N_ω , NY , and NZ . These last two register values above which the collocation oscillatory solution was found to be stable up to at least three significant figures within the ranges checked. In order to illustrate the oscillatory collocation solution behavior respect to NY and NZ , Figs. 4 to 6 show six different sets of collocation parameters for $C = 0.05$, $N_\omega = 10^3$, $M = 10^4$, $t = 0-9\pi/12$ Rads. While time elapses the numeric collocation solution could vary greatly before reaching stability with increasing values of collocation parameters, more so regarding the Hartmann wall layer velocity profiles than the side wall layer ones. This is expected since the side wall layer width is estimated to be $O(M^{-1/2})$ while

Hartmann wall layer width is $O(M^{-1})$, i. e., $\delta_L > \delta_H$, as discussed in Cuevas (1994). It can also be seen that the region of interest for the side wall layer velocity profiles is approximately the final 15% of the duct transversal length, where differences between solutions are clearly noticeable, specially at Fig. 6 (left). In contrast, for the Hartmann wall layer velocity profiles the region of interest is approximately the final 3% of the duct transversal length, as noticeable in Figs. 4 (right), 5 (right), and 6 (right). It can be distinguished as well that collocation solutions with $NY = NZ = 15, 45$, and 75 are not stable yet for the Hartmann wall layer definition, this particularly shown again in Figs. 4 (right), 5 (right), and 6 (right) in the close vicinity of $y = 1$. Now, solutions with $NY = NZ = 125, 180$, and 210 have ceased to oscillate between adjacent collocation points. This advices to carefully establish collocation parameters when searching for

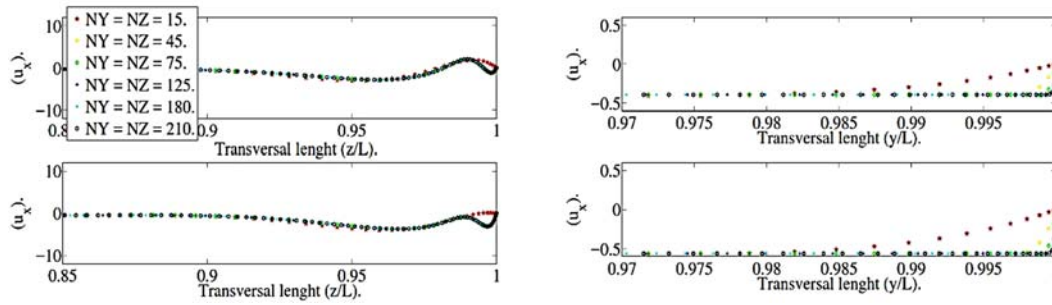


Fig. 6. Numerical solution respect to collocation parameters. $C = 0.05, N_\omega = 10^3, M = 10^4, M / N_\omega = 10. t = 8\pi / 12$ (top) and $9\pi / 12$ (Bottom)Rads. Left: profiles at $y = 0$. Right: profiles at $z = 0$.

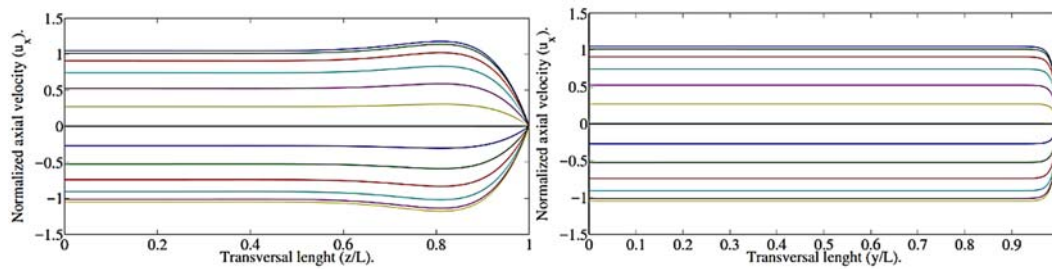


Fig. 7. Left: velocity profiles at plane $y = 0$. Right: velocity profiles at plane $z = 0$. $C = 0.01, N_\omega = 10^5, M = 10^2; M / N_\omega = 10^{-3}$.

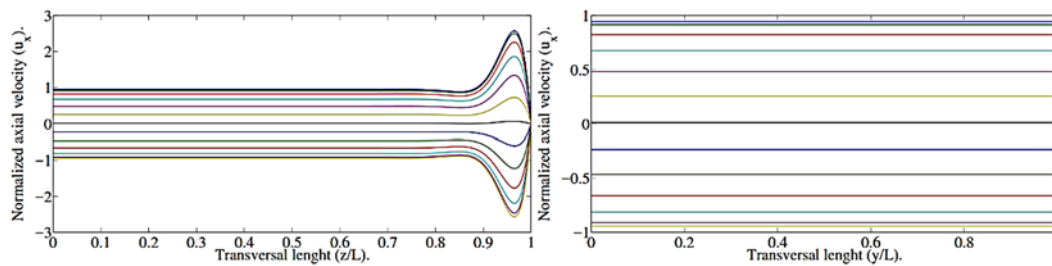


Fig. 8. Left: velocity profiles at plane $y = 0$. Right: velocity profiles at plane $z = 0$. $C = 0.01, N_\omega = 10^4, M = 10^3; M / N_\omega = 10^{-1}$.

solutions since flow structure patterns could be entirely missed in the side wall layer by not employing enough collocation points, e. g., Fig. 6 (left). It must be noticed that with respect to the Hartmann wall layer, the subject would not be as much as of missing flow structure patterns due to not setting a sufficient number of collocation points, but of a correct profile resolution, e. g., Figs. 4 (right), 5 (right), and 6 (right). Profiles under previous discussion are shown over the time period $4\pi/12-9\pi/12$ Rads divided in increments of $\pi/12$ Rads. No other examples are shown here. Figs. 4 (left) to 6 (right) also serve the purpose of showing that flow structure patterns in the side wall layer could get a little more complex when compared to the steady case once MHD effects are established with its characteristic M-shaped profiles, back-flows and overshoots as thoroughly discussed in Cuevas (1994) and Cuevas *et al.* (1997). The main observation is that flow structure in the oscillatory

case for the side wall layer depends both on increasing M and M / N_ω . As M / N_ω ratio increases, it is noticeable in the figures how the flow bulk gets progressively located into the last 15-10% of the duct transversal length in spatial terms, while simultaneously flow structure shows increasing complexity in terms of different emerging flow patterns. On the other hand, for the same circumstances the Hartmann wall layer flow bulk is distributed over the entire duct transversal length except for the last 5-3%. Figs. 7 to 9 attempt to illustrate these last remarks by showing velocity profiles for both side and Hartmann wall layers over a semi-period ($t = 0 - \pi$ Rads) divided in increments of $\pi/12$ Rads for three cases of increasing M / N_ω ratio within the parametric ranges solved. In Fig. 7 with $M / N_\omega = 10^{-3}$, side wall layer velocity profiles have an smooth (i., e., not pronounced) M-shaped contour, but they progressively transition into a little

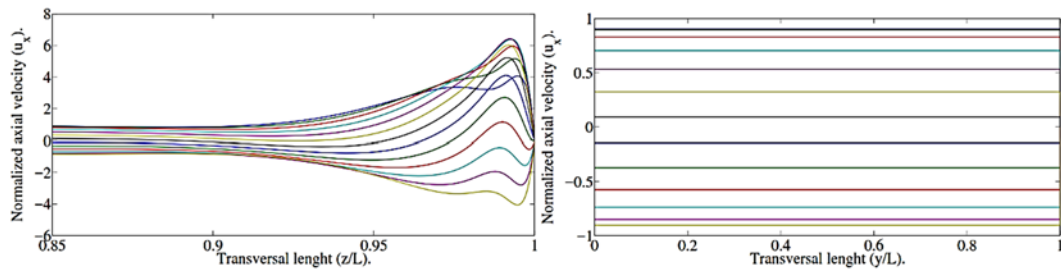


Fig. 9. Left: velocity profiles at plane $y = 0$. Right: velocity profiles at plane $z = 0$. $C = 0.01, N_\omega = 10^3$, $M = 10^4; M / N_\omega = 10^1$.

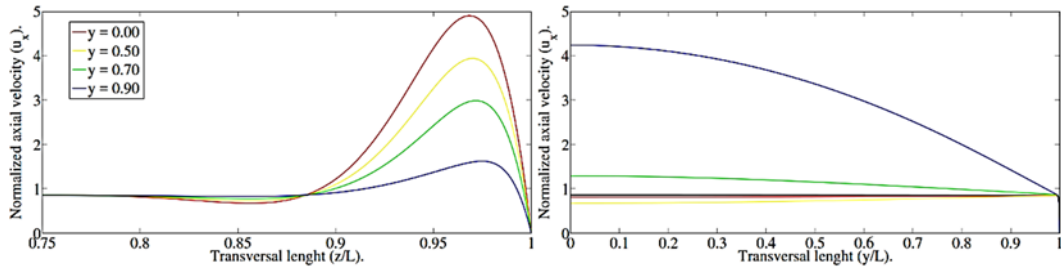


Fig. 10. Oscillatory collocation solution profiles at different planes. $C = 0.05, N_\omega = 10^4, M = 10^3$; $M / N_\omega = 10^{-1}, t = 0$ Rads. Left: side wall layer. Right: Hartmann wall layer.

more complicated shape as shown in Figs. 8 and 9, with $M / N_\omega = 10^{-1}$ (i., e., a more abrupt M-shaped contour in this case) and 10^1 (which can hardly be described as a M-shaped contour at all) respectively. Notice also how from (left) Figs. 7, 8, and 9, flow structure patterns keep getting closer and closer to the boundary at $z = 1$. At the same time, the time-step evolution for the Hartmann wall layer velocity profiles is much more less dynamic compared to their counterparts in the side wall layer, basically getting closer and closer to the boundary at $y = 1$ and not showing signs of emergence of different flow structure patterns as shown in (right) Figs. 7, 8, and 9.

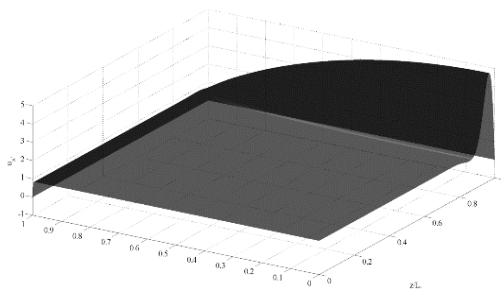


Fig. 11. 3-D velocity profile provided by the collocation solution. $C = 0.05, N_\omega = 10^5$, $M = 10^3; t = 0$ Rads.

Other aspects in need of illustration are the behavior of the oscillatory collocation solution respect to the plane of visualization longitudinal to the externally

applied magnetic field and the time-step evolution of the velocity profiles. Fig. 10 (left) shows how the oscillatory collocation solution matches the steady collocation case as portrayed in Cuevas (1994) for the set of parameters presented for the side wall layer. The Hartmann wall layer situation, absent in the discussion developed on Cuevas (1994), Cuevas *et al.* (1997) due to the use of the core-side-layer approximation, is shown here in Fig. 10 (right). Interestingly, it is as much as eventful as its counterpart, only that not in terms of emerging flow structure patterns but on the transitioning from flat slug-like velocity profiles and more parabolic shaped velocity profiles sharply cut towards the boundary at $y = a$. These remarks can be put in perspective aided by Fig. 11, which help us to explain the features just described. Figs. 12 to 14 show the behavior of velocity profiles respect to the plane of visualization while simultaneously present a grasp on their time-step evolution for $M = 10^4$, in order to show how flow structure develops over time for this relatively high Hartmann number. Other cases are not shown due to space constraints. Profiles are illustrated over a semi-period ($0 - \pi$ Rads) divided in increments of $2\pi/12$ Rads. As commented, in this problem we are not dealing with the transient solution but with the steady-state or long run oscillatory one. Because of that no initial conditions were set when calculating the solution, so at $t = 0$ Rads, the velocity profiles time-step evolution begin not at their maximum normalized values for the time set solved, which are reached at Fig. 12 (right, top) for the side wall layer and Fig. 14 (right, bottom) for the Hartmann wall layer case. For the side wall layer, right at a half of the semi-period ($t = 6\pi/12$ Rads) the velocity is already reversing its

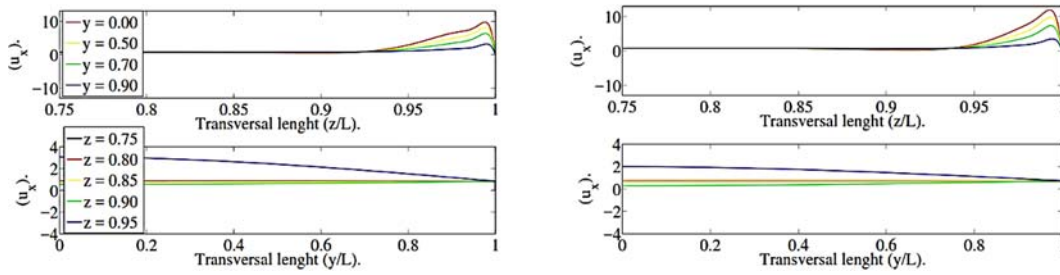


Fig. 12. Collocation solution profiles at different planes/time-step evolution. $C = 0.05, N_\omega = 10^3$, $M = 10^4$; $M / N_\omega = 10^1$. Left: $t = 0$ Rads. Right: $t = 2\pi/12$ Rads.

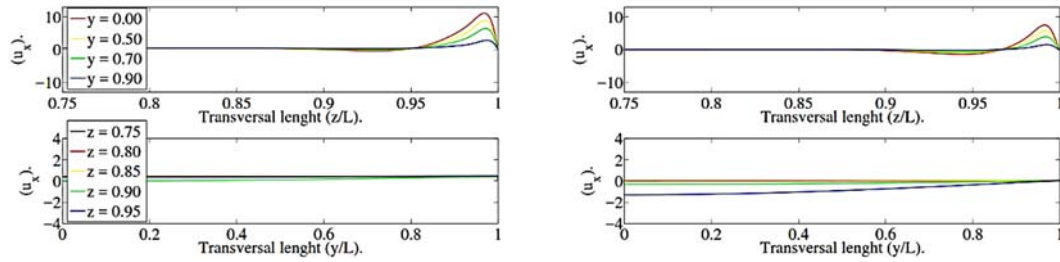


Fig. 13. Collocation solution profiles at different planes/time-step evolution. $C = 0.05, N_\omega = 10^3$, $M = 10^4$; $M / N_\omega = 10^1$. Left: $t = 4\pi/12$ Rads. Right: $t = 6\pi/12$ Rads.

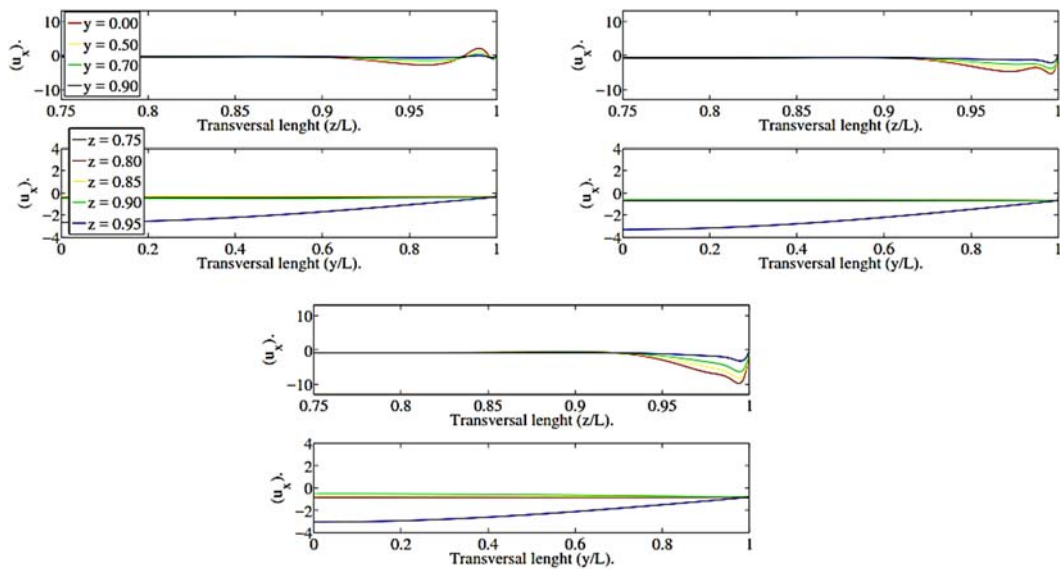


Fig. 14. Collocation solution profiles at different planes/time-step evolution. $C = 0.05, N_\omega = 10^3$, $M = 10^4$; $M / N_\omega = 10^1$. Left: $t = 4\pi/12$ Rads. Right: $t = 6\pi/12$ Rads.

direction, as shown in Fig. 13 (right, top). Flow structure remains pretty much the same, somewhat resembling an smoothly serrated M-shape with apparition of some back-flow as noticeable in the same figure and also in Fig. 14 (top, left). As time elapses, the back-flow shown at Fig. 13 (right, top) keeps increasing along the new flow direction, while the overshoot in the same figure keeps diminishing as shown in Fig. 14 (top, right), and (bottom). This continues to happen until flow structure develops

into what is shown in Fig. 14 (bottom, top); two valleys and two peaks in the negative direction, each one more pronounced towards the duct boundary. That is, the flow continues to evolve to form again what was described as an smoothly serrated M-shape of Fig. 12 (left, top). The velocity completely reverses and begins to establish the same time-step evolution pattern for the other half of the semi-period, which is not shown here. Figs. 12 to 14 also show the behavior of the oscillatory collocation

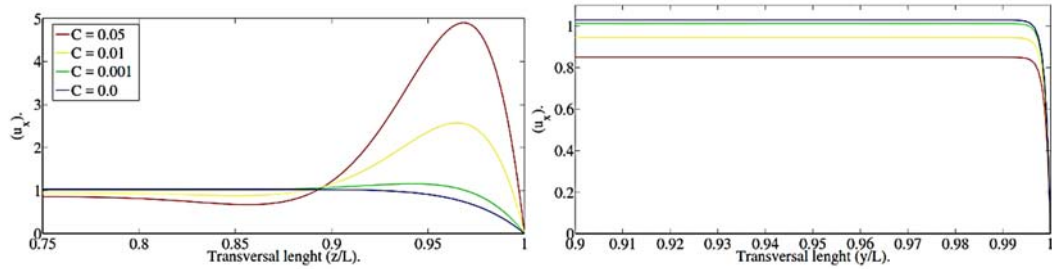


Fig. 15. Collocation solution profiles respect to wall conductance parameter. $N_\omega = 10^6$, $M = 10^3$; $M / N_\omega = 10^{-3}$, $t = 0$ Rads. Left: profiles at $y = 0$. Right: profiles at $z = 0$.

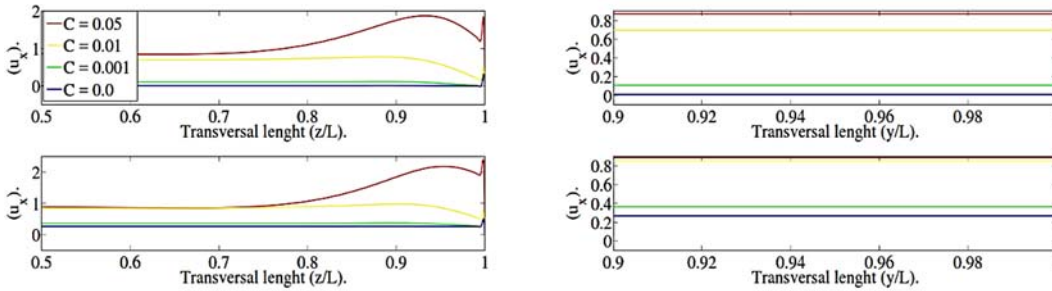


Fig. 16. Collocation solution profiles respect to wall conductance parameter. $N_\omega = 10^2$, $M = 10^4$, $M / N_\omega = 10^2$, $t = 0 \wedge \pi/12$ Rads. Left: profiles at $y = 0$. Right: profiles at $z = 0$.

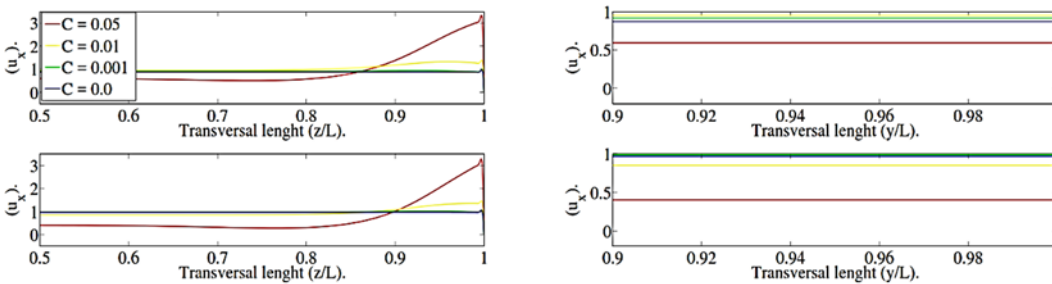


Fig. 17. Collocation solution profiles respect to wall conductance parameter. $N_\omega = 10^2$, $M = 10^4$, $M / N_\omega = 10^2$, $t = 4\pi/12 \wedge 5\pi/12$ Rads. Left: profiles at $y = 0$. Right: profiles at $z = 0$.

solution velocity profiles at different visualization planes ($0 < y < a$), presenting their correct differentiation respect their individual relative proximity to the boundary $y = a$ and its non slip condition. Due that condition, profiles at different planes present the same basic shape but more and more attenuated as they get closer towards the boundary.

Another feature to take into account is the behavior of the oscillatory collocation solution respect to the wall con ductance parameter (\mathbb{C}). Fig. 15 (left) shows how the solution is also in good agreement with the steady collocation solution case as reported in Cuevas (1994), Cuevas *et al.* (1997). Fig. 15 (right) shows the situation for the Hartmann wall layer which as commented is absent in those references due to the core-side-layer approximation. Notice that calculations for $\mathbb{C} = 0.001$ were performed too in order to further portrait the

transition to the isolating duct wall case ($\mathbb{C} = 0.0$) Figs. 16 to 19 present the behavior of the oscillatory collocation solution respect to \mathbb{C} and its time-step evolution for both side and Hartmann wall layers velocity profiles. No other cases are shown here. Side wall layer velocity profiles with $\mathbb{C} \neq 0.0$ exhibit a basic structure shape thorough almost the entire semi-period, which in this particular case of parameters can be described as an smoothed M-shape with an small peak towards the boundary $z = 1$; peak which gets smaller and smaller with diminishing values of \mathbb{C} . That basic shape does not dramatically change for each value of \mathbb{C} but for the appearance of a progressive back-flow. For $\mathbb{C} = 0.001$ it can be only appreciated by the end of the semi-period in Fig. 19 (left, top) as well as the formation of a second valley or back-flow when the initial peak towards the boundary reverses its direction (appreciated in incipience in Fig. 19 (left,

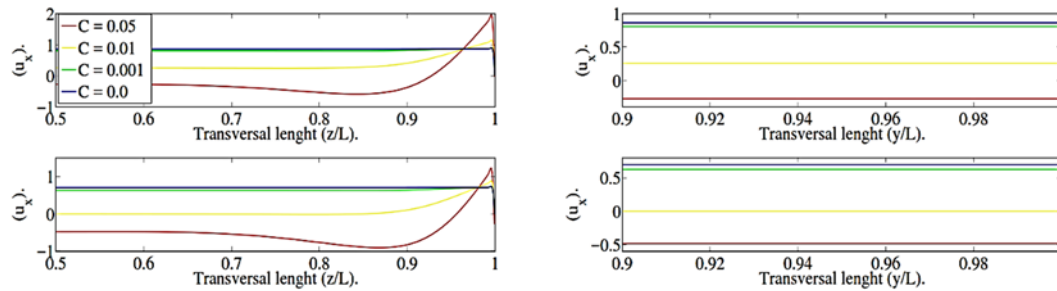


Fig. 18. Collocation solution profiles respect to wall conductance parameter. $N_\omega = 10^2$, $M = 10^4$, $M / N_\omega = 10^2$, $t = 8\pi/12 \wedge 9\pi/12$ Rads. Left: profiles at $y = 0$. Right: profiles at $z = 0$.

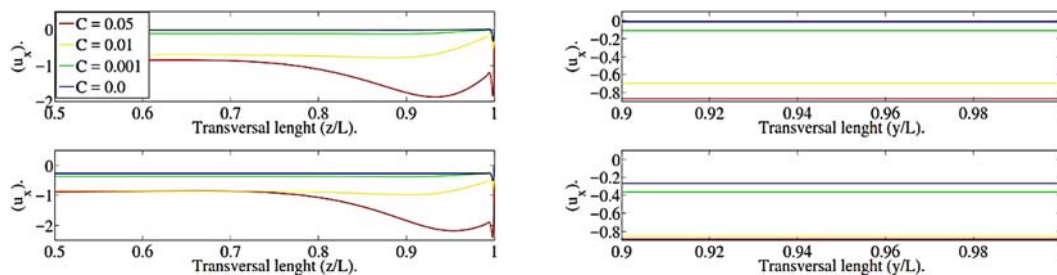


Fig. 19. Collocation solution profiles respect to wall conductance parameter. $N_\omega = 10^2$, $M = 10^4$, $M / N_\omega = 10^2$, $t = 12\pi/12 \wedge 13\pi/12$ Rads. Left: profiles at $y = 0$. Right: profiles at $z = 0$.

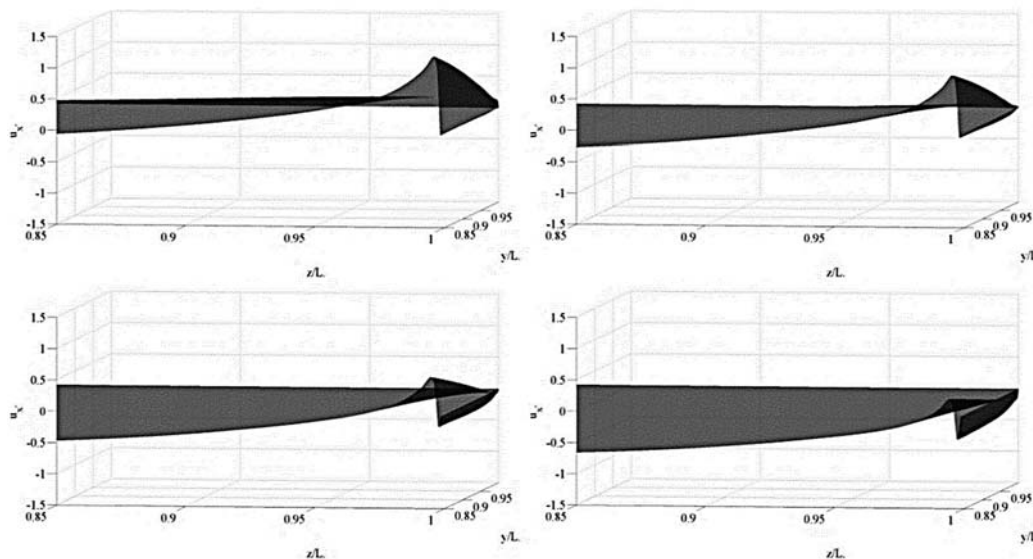


Fig. 20. Sample of 3 – D velocity profiles time-step evolution by the collocation solution. $C = 0.05, N_\omega = 10^2$, $M = 10^4$; $M / N_\omega = 10^2$. Left to right top: $t = 10\pi/32, 11\pi/32$ Rads, bottom: $t = 12\pi/32, 13\pi/32$ Rads.

bottom)). Notice how all along for $C = 0.0$ the case is different since no back-flow is present and the small peak towards the boundary at $z = 1$ is much more less pronounced. This kind of flow structure can be described as slug-like. For the Hartmann wall the velocity profiles and the entire situation is much more uneventful in terms of flow structure, limiting itself to cleaner slug-like patterns (i. e., no peaks towards the boundary $y = 1$). Complementarily, Figs. 20 and 21 try to further detail visualization on the

occurrence of back-flow by showing a sample of the 3D velocity profile time-step evolution for $C = 0.05$, conductivity for which the phenomena is more pronounced in this particular example.

Other characteristic to consider in this paper is the flow behavior with respect to varying Hartmann number value (M), parameter which corresponds to the externally applied magnetic field intensity. This is illustrated in Figs. 22 to 24 for three conductance

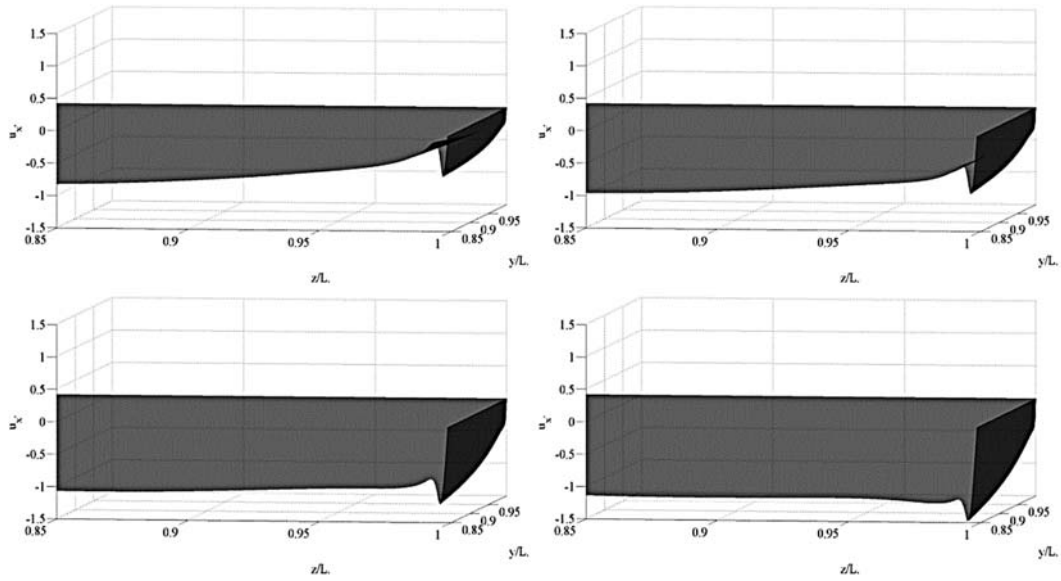


Fig. 21. Sample of 3 – D velocity profiles time-step evolution by the collocation solution. $C = 0.05$, $N_{\omega} = 10^5$, $M = 10^3$; $M / N_{\omega} = 10^2$. Left to right top: $t = 14\pi/32, 15\pi/32$ Rads, bottom: $t = 16\pi/32, 17\pi/32$ Rads.

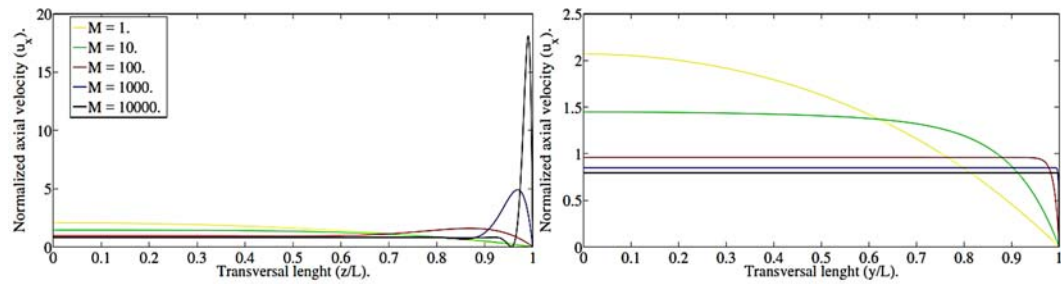


Fig. 22. Collocation solution respect to the Hartmann number. Left: profiles at $y = 0$. Right: profiles at $z = 0$. $C = 0.05, N_{\omega} = 10^6, t = 0$ Rads.

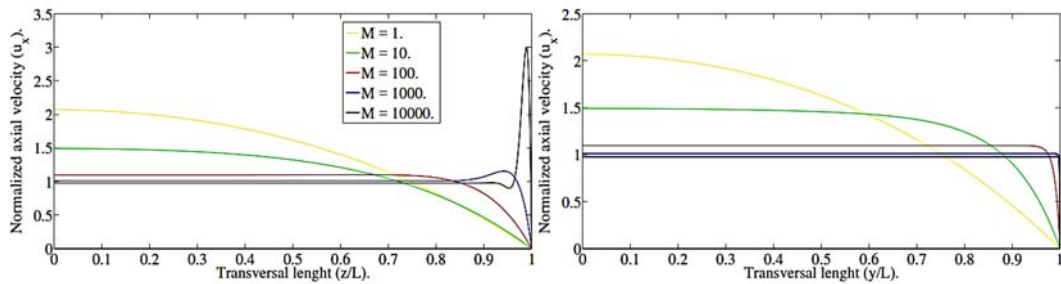


Fig. 23. Collocation solution respect to the Hartmann number. Left: profiles at $y = 0$. Right: profiles at $z = 0$. $C = 0.05, N_{\omega} = 10^6, t = 0$ Rads.

ratio values ($C = 0.05, 0.001$, and 0). As seen, profiles at $t = 0$ Rads match the features described in Cuevas (1994), Cuevas *et al.* (1997) for the steady case. No additional figures with different points in time at the time-step numerically solved are shown here. Notice particularly how for increasing M values the peak velocity value also increases sharply while the side layer thickness

decreases as expected. For $M = 10^3$ and $C \neq 0$, the peak velocity value is around 30% of its value with $M = 10^4$ due to the side layer velocity being $O(M^{1/2})$. Correspondingly, the side layer thickness is $O(M^{-1/2})$. As for $C = 0$, since in that case the induced electric currents totally close within the

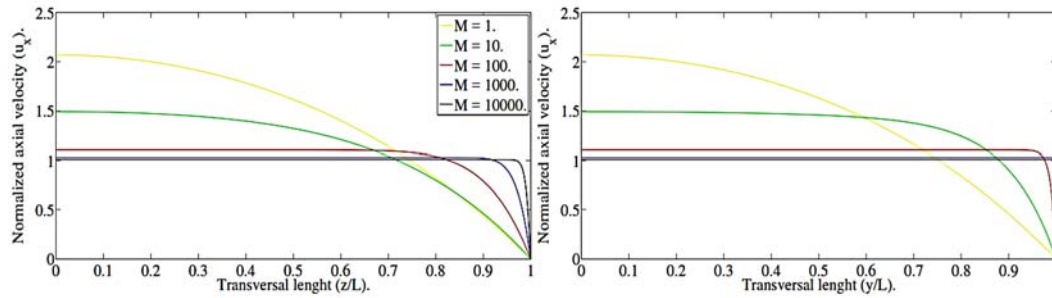


Fig. 24. Collocation solution respect to the Hartmann number. Left: profiles at $y = 0$. Right: profiles at $z = 0$. $C = 0.0, N_\omega = 10^6, t = 0$ Rads.

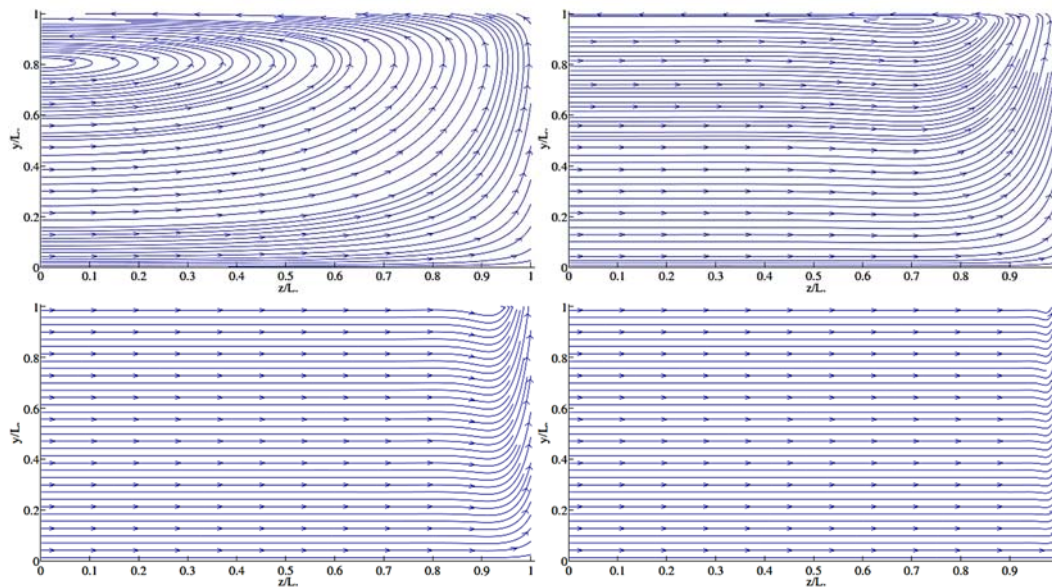


Fig. 25. Electric current surface density (\vec{j}) respect to the Hartmann number. Top left: $M = 10^1$, top right: $M = 10^2$, bottom left: $M = 10^3$, bottom right: $M = 10^4$. $C = 0.05, N_\omega = 10^6, t = 0$ Rads.

fluid and through the Hartmann layers, that circumstance seriously dampens any possible velocity overshoots and the side layer velocity results now of $O(1)$, as shown in Fig. 24 (left).

It's also interesting for the scope of this paper to briefly inquire on the induced electric current surface density (\vec{j}) distribution over the duct. The present configuration would be equivalent to an open circuit liquid-metal generator with a single wall conductance parameter, by no means an efficient setup for electric generation purposes. A more suitable generator-like setup would consider $C_H = 0, C_L \rightarrow \infty$, coupled with an adequate physical/numerical model for the attachment of a load resistance between the side walls. Those conditions fall within the feasibility of this present formulation. Mentioned inquiry was performed in Figs. 25 to 27 for wall conductance parameters (C) values of 0.05, 0.001, and 0. It is noticeable how as C gets near to 0 and M increments, more and more of the electric current lines close within the

increasingly thinner Hartmann layer in the fluid region. Extreme cases for this parametric situation are shown in Fig. 25 (top left) and Fig. 27 (bottom right). For a given $C \neq 0$ value the trend to notice is pretty much the same: increasing M values mean thinner Hartmann layers for electric current return and augmented closing of electric current lines within the conducting walls, for both side and Hartmann walls (Figs. 25 and 26). In the case of $C = 0$, the situation is defined by thinner and thinner Hartmann layers with the increment of M , since all electric current lines must close within the fluid region (Fig. 27).

As illustrated, relevant parameters to take into account regarding flow features and behavior with a given conductance parameter C are M, N_ω , and its ratio (M / N_ω). Numerical solutions for the oscillatory case were validated by comparison with an analytical oscillatory solution, finding good agreement (see again previous section). Behavior and features of the numerical collocation oscillatory

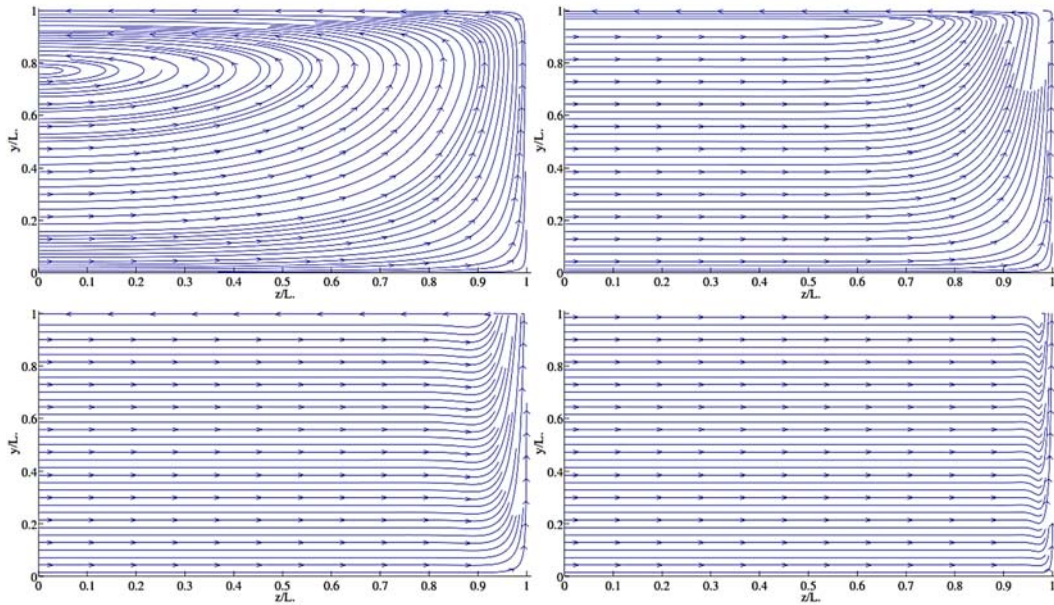


Fig. 26. Electric current surface density (\vec{j}) respect to the Hartmann number. Top left: $M = 10^1$, top right: $M = 10^2$, bottom left: $M = 10^3$, bottom right: $M = 10^4$. $C = 0.001$, $N_\omega = 10^6$, $t = 0$ Rads.

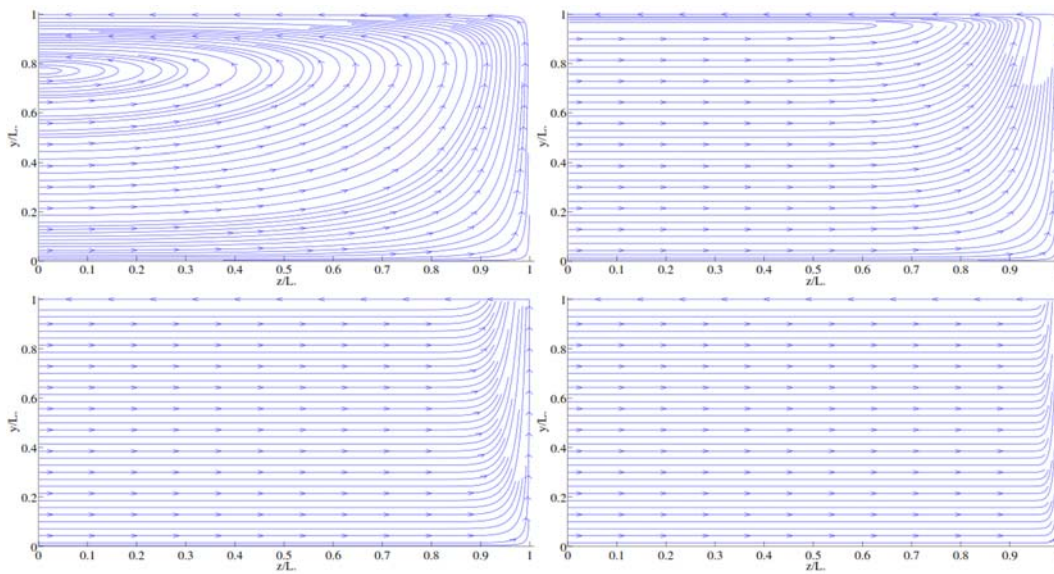


Fig. 27. Electric current surface density (\vec{j}) respect to the Hartmann number. Top left: $M = 10^1$, top right: $M = 10^2$, bottom left: $M = 10^3$, bottom right: $M = 10^4$. $C = 0.0$, $N_\omega = 10^6$, $t = 0$ Rads.

solution with respect to several parameters were inquired as follows: varying number of collocation points (N_Y , N_Z) and time-step profile evolution, see Figs. 4 to 6; varying M / N_ω ratio, see Figs. 7 to 9; different planes of visualization, see Fig. 10 and 11, different planes of visualization and time-step profile evolution, see Figs. 13 to 14; different wall conductance parameter values (C), see Fig. 15 (left) and (right); different wall conductance parameter values (C) and time-step velocity profile evolution, see Figs. 16 to 19; varying Hartmann number value

(M), see Figs. 22 to 24; and electric current surface density (\vec{j}) behavior with respect to wall conductance parameter (C) and Hartmann number (M), see Figs. 25 to 27.

6. CONCLUSION

A harmonically-driven, incompressible, electrically conducting, laminar, completely developed, and viscous flow through a thin walled duct of rectangular cross section interacting with a

uniform magnetic field traverse to its motion (axial) direction was numerically investigated under the inductionless approach. An estimation of the amount of current flowing through the Hartmann layers was provided in order to propose thin conducting boundary conditions at top/bottom walls to be able to include the insulating case. In this approximation the Hartmann layers were considered as return paths for the electric currents and numerically solved. Concordance between oscillatory analytical and present numerical calculations was established by revisiting a classic analytic asymptotic solution restricted to large Hartmann numbers in Mandal (1969). A non restricted oscillatory analytical solution absent in that reference was provided and compared to present numerical calculations, finding reasonable agreement. Several MHD features of the liquid metal oscillatory flow were explored in a parametric range of interest related to liquid metal magnetohydrodynamic alternating power generation applications. Influence over the velocity profiles of parameters such as wall conductance ratio (C), Hartmann number (M), and oscillatory interaction parameter (N_ω) was studied. It was found that emerging side layer and close vicinity flow structures/patterns depend mainly on the Hartmann number and oscillatory interaction parameter ratio (M / N_ω), while the situation for the Hartmann layer and close vicinity was in contrast less eventful. Increasing values of M / N_ω ratio are associated to complexer (in terms of generally more serrated in shape) flow structures/patterns towards the boundary in the side wall layer velocity profiles. At the same time, increasing M / N_ω ratios relate to thinner and thinner Hartmann layers with flow structures/patterns remaining practically unchanged. A comparable feature has been discussed in the literature for the steady case and served as partial rationale for developing the composite core-side-layer approximation in order to study the magnetohydrodynamics of steady liquid metal flows usable in direct power generation applications, but hadn't been illustrated for neither the former or the present oscillatory case (see again Cuevas (1994), Cuevas *et al.* (1997)). In this present study the core-side-layer approximation was not taken and therefore a broader analysis was conducted on liquid metal oscillatory (i., e., unsteady) flows usable in alternating electric power generation contexts. That kind of analysis was absent from the literature in the parametric ranges proposed here. Hence, calculations here presented conform, elaborate, and expand on what was presented in those references for the steady flow situation since now the analysis is performed on the non approximated oscillatory case. On the other hand, in terms of potential practical applicability the system here described represents a liquid metal magnetohydrodynamic generator functioning in an unoptimized open circuit configuration. Consequently, these calculations set the first steps towards the numerical investigation on the performance of a

cartesian-symmetric liquid metal MHD generator. In a first approximation that would require considering $C_H = 0, C_L \rightarrow \infty$ and the attachment of a load resistance to the setup here described in order to calculate its isotropic efficiency, things which are well within the feasibility of the formulation developed.

ACKNOWLEDGMENTS

The author expresses his gratitude to the Consejo Nacional de Ciencia y Tecnología (CONACYT) for its financial support in the form of a scholarship throughout the duration of his Ph. D. program conducted at CICATA-IPN, Santiago de Querétaro, Querétaro, México.

REFERENCES

- Akyüz, A. and M. Sezer (2003). Chebyshev polynomial solutions of systems of high-order linear differential equations with variable coefficients. *Applied mathematics and computation* 144(2), 237-247.
- Akyüz-Daşcıoğlu, A. and M. Sezer (2005). Chebyshev polynomial solutions of systems of higher-order linear fredholm–volterra integro-differential equations. *Journal of the Franklin Institute* 342(6), 688-701.
- Barrett, K. (2001). Duct flow with a transverse magnetic field at high hartmann numbers. *International journal for numerical methods in engineering* 50(8), 1893-1906.
- Bozkaya, C. and M. Tezer-Sezgin (2006). Boundary element solution of unsteady magnetohydrodynamic duct flow with differential quadrature time integration scheme. *International Journal for Numerical Methods in Fluids* 51(5), 567-584.
- Bozkaya, C. and M. Tezer-Sezgin (2007). Fundamental solution for coupled magnetohydrodynamic flow equations. *Journal of computational and applied mathematics* 203(1), 125-144.
- Bozkaya, N. and M. Tezer-Sezgin (2008). Time-domain BEM solution of convection–diffusion-type mhd equations. *International journal for numerical methods in fluids* 56(11), 1969-1991.
- Carabineanu, A., A. Dinu and I. Oprea (1995). The application of the boundary element method to the magnetohydrodynamic duct flow. *Zeitschrift für angewandte Mathematik und Physik ZAMP* 46(6), 971-981.
- Çelik, İ. (2005a). Approximate calculation of eigenvalues with the method of weighted residuals–collocation method. *Applied mathematics and computation* 160(2), 401-410.
- Çelik, İ. (2005b). Approximate computation of eigenvalues with chebyshev collocation method. *Applied mathematics and computation* 168(1), 125-134.

- Çelik, İ. (2006). Collocation method and residual correction using chebyshev series. *Applied mathematics and computation* 174(2), 910-920.
- Çelik, İ. (2011). Solution of magnetohydrodynamic flow in a rectangular duct by chebyshev collocation method. *International journal for Numerical methods in Fluids* 66(10), 1325-1340.
- Çelik, İ. and G. Gokmen (2005). Approximate solution of periodic sturm-liouville problems with chebyshev collocation method. *Applied mathematics and computation* 170(1), 285-295.
- Chang, C. C. and T. S. Lundgren (1961). Duct flow in magnetohydrodynamics. *Zeitschrift für angewandte Mathematik und Physik ZAMP* 46(6), 971-981. 12(2), 100-114.
- Cuevas, S. (1994). *Liquid-metal flow and heat transfer under strong magnetic fields*. Ph. D. thesis. 9-83.
- Cuevas, S., B. F. Picologlou, J. S. Walker and G. Talmage (1997). Liquid-metal mhd flow in rectangular ducts with thin conducting or insulating walls: laminar and turbulent solutions. *International journal of engineering science* 35(5), 485-503.
- Dehghan, M. and D. Mirzaei (2009). Meshless local boundary integral equation (LBIE) method for the unsteady magnetohydrodynamic (MHD) flow in rectangular and circular pipes. *Computer Physics Communications* 180(9), 1458-1466.
- Demendy, Z. and T. Nagy (1997). A new algorithm for solution of equations of MHD channel flows at moderate hartmann numbers. *Acta mechanica* 123(1-4), 135-149.
- Gardner, L. and G. Gardner (1995). A two dimensional bi-cubic b-spline finite element: used in a study of MHD-duct flow. *Computer methods in applied mechanics and engineering* 124(4), 365-375.
- Hunt, J. C. R. (1965). Magnetohydrodynamic flow in rectangular ducts. *Journal of Fluid Mechanics* 21(04), 577-590.
- Hunt, J. C. R. and K. Stewartson (1965). Magnetohydrodynamic flow in rectangular ducts. II. *Journal of fluid mechanics* 23(03), 563-581.
- Keşan, C. (2003). Chebyshev polynomial solutions of second-order linear partial differential equations. *Applied mathematics and computation* 134(1), 109-124.
- Liu, H. W. and S. P. Zhu (2002). The dual reciprocity boundary element method for magnetohydrodynamic channel flows. *The Anziam Journal* 44(02), 305-322.
- Mandal, K. (1968). Magnetohydrodynamic flow through a rectangular duct due to a periodic pressure gradient. *Applied Scientific Research* 19(1), 97-110.
- Mandal, K. (1969). Magnetohydrodynamic flow through a rectangular duct due to a periodic pressure gradient-II. *Applied Scientific Research* 21(1), 1-12.
- Mehmood, A. and A. Ali (2007). The effect of slip condition on unsteady MHD oscillatory flow of a viscous fluid in a planer channel. *Romanian journal of physics* 52(1/2), 85.
- Nesliturk, A. and M. Tezer-Sezgin (2005). The finite element method for mhd flow at high hartmann numbers. *Computer methods in applied mechanics and engineering* 194(9), 1201-1224.
- Nesliturk, A. and M. Tezer-Sezgin (2006). Finite element method solution of electrically driven magnetohydrodynamic flow. *Journal of computational and applied mathematics* 192(2), 339-352.
- Sezer, M. and M. Kaynak (1996). Chebyshev polynomial solutions of linear differential equations. *International Journal of Mathematical Education in Science and Technology* 27(4), 60F7-618.
- Shakeri, F. and M. Dehghan (2011). A finite volume spectral element method for solving magnetohydrodynamic (MHD) equations. *Applied Numerical Mathematics* 61(1), 1-23.
- Shercliff, J. A. (1953). Steady motion of conducting fluids in pipes under transverse magnetic fields. In *Mathematical Proceedings of the Cambridge Philosophical Society* 49, Cambridge Univ Press.
- Singh, B. and J. Lal (1978). Magnetohydrodynamic axial flow in a triangular pipe under transverse magnetic field. *Indian J. Pure Appl. Math.* 9, 101-115.
- Singh, B. and J. Lal (1979). MHD axial flow in a triangular pipe under transverse magnetic field parallel to a side of the triangle. *Indian J. of Technology* 17, 184-189.
- Singh, B. and J. Lal (1984). Finite element method for unsteady MHD flow through pipes with arbitrary wall conductivity. *International journal for numerical methods in fluids* 4(3), 291-302.
- Singh, B. and P. Agarwal (1984). Numerical solution of a singular integral equation appearing in magnetohydrodynamics. *Zeitschrift für angewandte Mathematik und Physik ZAMP* 35(6), 760-770.
- Tezer-Sezgin, M. (1994). Boundary element method solution of MHD flow in a rectangular duct. *International journal for numerical methods in fluids* 18(10), 937-952.
- Tezer-Sezgin, M. and S. H. Aydin (2002). Dual reciprocity boundary element method for magnetohydrodynamic flow using radial basis functions. *International Journal of Computational Fluid Dynamics* 16(1), 49-63.
- Tezer-Sezgin, M. and S. H. Aydin (2006). Solution

of magnetohydrodynamic flow problems using the boundary element method. *Engineering analysis with boundary elements* 30(5), 411-418.

Tezer-Sezgin, M. and S. Köksal (1989). Finite element method for solving MHD flow in a rectangular duct. *International journal for numerical methods in engineering* 28(2), 445-459.

APPENDIX A. ANALYTICAL DETAILS

Equation to be solved is:

$$\frac{\partial \bar{u}}{\partial t} + (\bar{u} \cdot \nabla) \bar{u} = -\frac{1}{\rho} \nabla p + \nu \nabla^2 \bar{u} + \frac{\bar{j} \times \bar{B}}{\rho} \quad (30)$$

Considering

$$\bar{u} = \bar{u}(y, z, t) \hat{e}_x, \quad \phi = \phi(y, z, t), \quad \bar{B} = \bar{B}_0 + \bar{b} \approx \bar{B}_0$$

(inductionless approximation), $\bar{B} = B_0 \hat{y}$, and using the Ohm's law in the gradient formulation ($\bar{j} = \sigma(-\nabla \phi + \bar{u} \times \bar{B})$), Eq. (30) turns into:

$$\frac{\partial u}{\partial t} = -\frac{1}{\rho} \nabla p + \nu \left[\frac{\partial^2 u}{\partial y^2} + \frac{\partial^2 u}{\partial z^2} \right] + \sigma \frac{B_0}{\rho} \frac{\partial \phi}{\partial z} - \sigma \frac{B_0^2}{\rho} u \quad (31)$$

Now, combining $\nabla \cdot \bar{j} = 0$ with Ohm's law, one gets:

$$\frac{\partial^2 \phi}{\partial y^2} + \frac{\partial^2 \phi}{\partial z^2} - B_0 \frac{\partial u}{\partial z} = 0 \quad (32)$$

Eqs. (31) and (32) constitute the system to solve in the gradient formulation. Next we define the dimensionless variables

$$\tilde{B} = B / B_0 = 1, \quad \tilde{u} = u / u_0^*, \quad \tilde{t} = \omega t, \quad \tilde{y} = y / L,$$

$\tilde{z} = z / L, \quad \tilde{d} = d / L, \quad \partial \tilde{p} / \partial \tilde{x} = \tilde{G} e^{it},$ (\tilde{G} being the pressure gradient amplitude). Dropping tildes and considering only dimensionless quantities from now on, they change into:

$$N_\omega^{-1} \frac{\partial u}{\partial t} = -\frac{\partial p}{\partial x} + M^{-2} \left[\frac{\partial^2 u}{\partial y^2} + \frac{\partial^2 u}{\partial z^2} \right] + \frac{\partial \phi}{\partial z} - u \quad (33)$$

$$\frac{\partial^2 \phi}{\partial y^2} + \frac{\partial^2 \phi}{\partial z^2} - \frac{\partial u}{\partial z} = 0 \quad (34)$$

Eqs. (33) and (34) would now constitute a restatement of the system to solve. Proposing $u = u_0(y, z) e^{it}$, and $\phi = \phi_0(y, z) e^{it}$, they conduce to a particularization of the problem for its spatial part as:

$$M^{-2} \left[\frac{\partial^2 u_0}{\partial y^2} + \frac{\partial^2 u_0}{\partial z^2} \right] - (1 - iN_\omega^{-1}) u_0 = G - \frac{\partial \phi_0}{\partial z} \quad (35)$$

$$\frac{\partial^2 \phi_0}{\partial y^2} + \frac{\partial^2 \phi_0}{\partial z^2} - \frac{\partial u_0}{\partial z} = 0 \quad (36)$$

With spatial boundary conditions for isolating and perfectly conducting side and Hartmann walls (respectively) given by:

$$u_0(y = \pm a; z) = \phi_0(y = \pm a; z) = 0 \quad (37)$$

$$u_0(y; z = \pm 1) = \frac{\partial \phi_0}{\partial z}(y; z = \pm 1) = 0 \quad (38)$$

Eqs. (35) and (36) subject to boundary conditions given by Eqs. (37) and (38) can be solved by means of applying a suitable variables separation. This begins by making ourselves sure that solutions for $u = u_0(y, z)$ and $u = \phi_0(y, z)$ in the following form satisfy the boundary conditions, given firstly by Eqs. (38):

$$u_0(y, z) = \sum_{n=0}^{\infty} u_n(y) \text{Cos}(\alpha_n z) \quad (39)$$

$$\phi_0(y, z) = \sum_{n=0}^{\infty} \phi_n(y) \text{Sin}(\alpha_n z) \quad (40)$$

Indeed they do, once considering that:

$$G(z) = G \sum_{n=0}^{\infty} a_n \text{Cos}(\alpha_n z) \quad (41)$$

With $\alpha_n = (2n + 1)\pi / 2, \alpha_n = 4(-1)^n / (2n + 1)\pi,$ and $n = 0, 1, 2, 3, \dots$

Replacing Eqs. (39) and (40) into (37) and (38), one obtains:

$$M^{-2} \frac{d^2 u_n(y)}{dy^2} - (M^{-2} \alpha_n^2 + \eta) u_n(y) + \alpha_n \phi_n(y) - G a_n = 0 \quad (42)$$

$$\frac{d^2 \phi_n(y)}{dy^2} - \alpha_n^2 \phi_n(y) + \alpha_n u_n(y) = 0 \quad (43)$$

With $\eta = 1 + iN_\omega^{-1}$. This last ordinary differential equations system is subject to the following boundary conditions:

$$u_n(\pm a) = \phi_n(\pm a) = 0 \quad (44)$$

Solutions for the system of Eqs. (42) and (43) subject to boundary conditions given by Eqs. (44) take the form:

$$u(x, y, z) = \frac{\delta e^{-y(\sqrt{\epsilon_1 + \sqrt{\epsilon_2}})}}{8\pi\gamma(2n+1)\epsilon} \left(e^{\zeta_1 y} (\epsilon_1((2\pi n + \pi)^2 - 2\epsilon_2) + 1) \text{sech}(a\zeta_2) + 4(2\pi n + \pi)^2 \epsilon e^{\zeta_2 y} \right)$$

$$-\varepsilon_2((2\pi n + \pi)^2 - 2\varepsilon_1)e^{\zeta_2 y}(e^{\sqrt{2}y\sqrt{\varepsilon_1}} + 1)\operatorname{sech}(a\zeta_1) \Big) \quad \zeta_2 = \sqrt{\varepsilon_2} / \sqrt{2}, \quad (45)$$

$$\phi_n(y) = \frac{\delta}{2\gamma\varepsilon} (2\varepsilon - \varepsilon_2 \operatorname{sech}(a\zeta_1)\cosh(\zeta_1 y) + \varepsilon_1 \operatorname{sech}(a\zeta_2)\cosh(\zeta_2 y)) \quad (46)$$

With

$$\beta = \eta M^2 + \alpha_n^2, \quad \gamma = (1 - \eta)M^2 \alpha_n^2 - \alpha_n^4, \quad \delta = GM^2 a_n \alpha_n, \quad \varepsilon = \sqrt{\beta^2 + 4\gamma}, \quad \varepsilon_1 = \beta - \varepsilon, \quad \varepsilon_2 = \beta + \varepsilon, \quad \zeta_1 = \sqrt{\varepsilon_1} / \sqrt{2}, \quad \text{and}$$

Final solutions are reconstructed by replacing solutions for $u_n(y)$ and $\phi_n(y)$ provided by Eqs. (45) and (46) into Eqs. (39) and (40) in order to find out $u_0(y, z)$ and $\phi_0(y, z)$. Once that's completed, one can put together $u = u_0(y, z)e^{it}$, $\phi = \phi_0(y, z)e^{it}$ as written in Eq. (29). Ultimately the velocity is normalized as proposed in Eq. (21) before visualization.